IOP Publishing Bioinspir. Biomim. 13 (2018) 045002 https://doi.org/10.1088/1748-3190/aabf4c

Bioinspiration & Biomimetics

PAPER

RECEIVED
27 November 2017

REVISED
26 March 2018

ACCEPTED FOR PUBLICATION
19 April 2018

PUBLISHED
30 May 2018

Flow interactions of two- and three-dimensional networked bio-inspired control elements in an in-line arrangement

Melike Kurt and Keith W Moored

Mechanical Engineering and Mechanics, Lehigh University, Bethlehem, PA 18015, United States of America

E-mail: mek514@lehigh.edu

Keywords: flying/swimming, collective performance, vortex-body interaction, fish schools, bio-inspired propulsion, experimental fluid dynamics

Abstract

We present experiments that examine the modes of interaction, the collective performance and the role of three-dimensionality in two pitching propulsors in an in-line arrangement. Both two-dimensional foils and three-dimensional rectangular wings of $AR = 2$ are examined. In contrast to previous work, two interaction modes distinguished as the coherent and branched wake modes are not observed to be directly linked to the propulsive efficiency, although they are linked to peak thrust performance and minimum power consumption as previously described (Boschitsch *et al* 2014 *Phys. Fluids* **26** 051901). In fact, in closely-spaced propulsors peak propulsive efficiency of the follower occurs near its minimum power and this condition reveals a branched wake mode. Alternatively, for propulsors spaced far apart peak propulsive efficiency of the follower occurs near its peak thrust and this condition reveals a coherent wake mode. By examining the collective performance, it is discovered that there is an optimal spacing between the propulsors to maximize the collective efficiency. For two-dimensional foils the optimal spacing of $X^* = 0.75$ and the synchrony of $\phi = 2\pi/3$ leads to a collective efficiency and thrust enhancement of 42% and 38%, respectively, as compared to two isolated foils. In comparison, for $AR = 2$ wings the optimal spacing of $X^* = 0.25$ and the synchrony of $\phi = 7\pi/6$ leads to a collective efficiency and thrust enhancement of 25% and 15%, respectively. In addition, at the optimal conditions the collective lateral force coefficients in both the two- and three-dimensional cases are negligible, while operating off these conditions can lead to non-negligible lateral forces. Finally, the peak efficiency of the collective and the follower are shown to have opposite trends with increasing spacing in two- and three-dimensional flows. This is correlated to the breakdown of the impinging vortex on the follower wing in three-dimensions. These results can aid in the design of networked bio-inspired control elements that through integrated sensing can synchronize to three-dimensional flow interactions.

1. Introduction

Many aquatic animals propel themselves by oscillating their fins in unsteady motions and quite often these animals organize into collectives or schools. Schools have inspired the imagination and with it a host of hypotheses for their function ranging from social behaviors [2] and enhanced protection against predators [3] to a reduction in the energetic cost of swimming [4]. Regardless of the prime function, animals in a collective encounter fluid dynamic interactions from their neighbors that may modify their locomotion energetics, force production or force them into a particular arrangement [5]. For example, idealized two-dimensional fish swimming in a side-by-side or biplane configuration can increase their thrust by as much as 50% [6–8]. Similarly, even an isolated fish can enhance its thrust production and improve its energetics by synchronizing its dorsal-caudal fin interactions [9, 10]. It has been further recognized that these schooling or fin–fin interactions are highly dependent upon the arrangement of fish or propulsors [4, 11], which can be decomposed into canonical in-line, side-by-side, or tip-to-tip arrangements. Most studies have examined one of the canonical arrangements, however, a few have begun to examine mixtures of these arrangements [12, 13] with some showing further performance improvements beyond the canonical arrangements. Nevertheless, here we will focus on the

canonical *in-line* arrangement of propulsors, which acts as a simple model of dorsal-caudal fin interactions where there is a follower directly downstream of a leader.

Our current understanding of in-line interactions that occur among fish in a school or between the fins on a single fish are mostly limited to two-dimensional flows [1, 12, 14–18] where the phase difference or synchrony of propulsors and the spacing have been identified as the major parameters affecting performance. For example, Gopalkrishnan *et al* [14] examined the interaction between a heaving and pitching airfoil and the vortices shed from a D-section cylinder. Their results indicated that depending upon the synchrony between the impinging vortices and the airfoil motion, interaction modes emerged that correlated with peak propulsive performance. Similarly, Drucker and Lauder [9] revealed the flow interactions between the dorsal and caudal fins on teleost fish by using particle image velocimetry (PIV). They hypothesized that, with the proper synchrony, this interaction could improve the thrust production of fish with little to no additional energetic cost. Consequently, Akhtar *et al* [15] confirmed this hypothesis with numerical simulations conducted on two heaving and pitching foils. By varying the synchrony they confirmed that the peak in thrust generation is associated with the formation of a leading-edge vortex on the follower foil at certain synchronies. Additionally, Rival *et al* [16] examined the forces and flowfields of in-line interactions between two heaving and pitching foils with a constant spacing by using a combination of numerical and experimental data. This parameter space was later extended to consider variations in both the sychrony and spacing in the numerical study of Broering *et al* [18] where is was discovered that the optimal synchrony varied with the foil spacing. Furthermore, these numerical findings on in-line foil interactions were confirmed and extended through an extensive experimental study [1]. In this study both the foil synchrony and spacing were altered where it was proposed that there were branched and coherent interaction modes linked to the troughs and peaks in the propulsive efficiency, respectively. More recently, Shoele and Zhu [12] numerically investigated the interactions of two foils in an in-line and side-by-side arrangement as well as three foils in a triangular formation. A performance enhancement was reported for all the arrangements, although the foils in the triangular formation were shown to perform poorly compared with the other arrangements. Finally, experimental studies have identified that the thrust and efficiency enhancement of in-line foils can be understood simply as alterations in the angle of attack of the follower foil leading to enhancements or degradations in the force production [19–21]. All of these studies advanced our knowledge of *two-dimensional* interactions among propulsors, however, far fewer studies have examined the *three-dimensional* interactions that occur between fins and in fish schools.

Force measurements on three-dimensional in-line interacting wings were examined in the context of an ornithopter vehicle [22]. By varying the synchrony and spacing of the wings it was determined that indeed thrust and efficiency could be enhanced as compared to isolated wings and, in contrast to two-dimensional studies, the optimal spacing was as close as possible. Yet, no flow field measurements were employed to explain the observed performance enhancements. More directly connected to swimmers, Daghooghi and Borazjani [23] conducted one of the first numerical studies investigating the role of three dimensionality on the propulsive performance and flow around schooling fish. They examined an infinite rectangular arrangement of swimmers operating with in-phase synchrony and discovered that the vortex wakes shed from a swimmer broke down into incoherent vorticity before impinging on a following swimmer. This led to little coherent vortical energy available for a follower to extract and improve its performance. More recently, the three-dimensional fin–fin interactions on jack fish have been examined numerically [24]. It was discovered that complex three-dimensional interactions among the dorsal fin trailing-edge vortices, the posterior body vortices and the leading-edge caudal fin vortices improve the caudal fin thrust and reduce the drag acting on the body. These studies highlight that only a small set of the three-dimensional interactions that occur in schools and fin–fin interactions have been probed. Moreover, studies examining the flow physics have only been investigated numerically and by using complex full-fish models.

Motivated by these studies, we present new two- and three-dimensional experiments that examine the in-line interactions between two propulsors. We consider two main questions: how does *three-dimensionality* alter our framework for understanding schooling interactions, and, as a model of the fin–fin interactions on a single swimmer, what is the *collective* performance of in-line propulsors? It is further discovered that coherent and branched interaction modes are *not* directly linked to the propulsive efficiency as previously proposed, but are indicative of peak thrust and minimum power conditions, respectively, in accordance with prior work [1].

2. Experimental setup and methods

The experiments were conducted in a closed loop, free-surface water tunnel with a test section length of 4.9 m, a width of 0.93 m, and a depth of 0.61 m. One flow speed of $U_\infty = 0.071$ m s^{-1} was used throughout all of the experiments giving a chord-based Reynolds number of 7500. Two water tunnel configurations were used in order to compare the performance and flow structures of two-dimensional hydrofoils and three-dimensional wings. In the two-dimensional configuration, a splitter plate and a surface plate were installed such that the wings would span the entire depth between the two

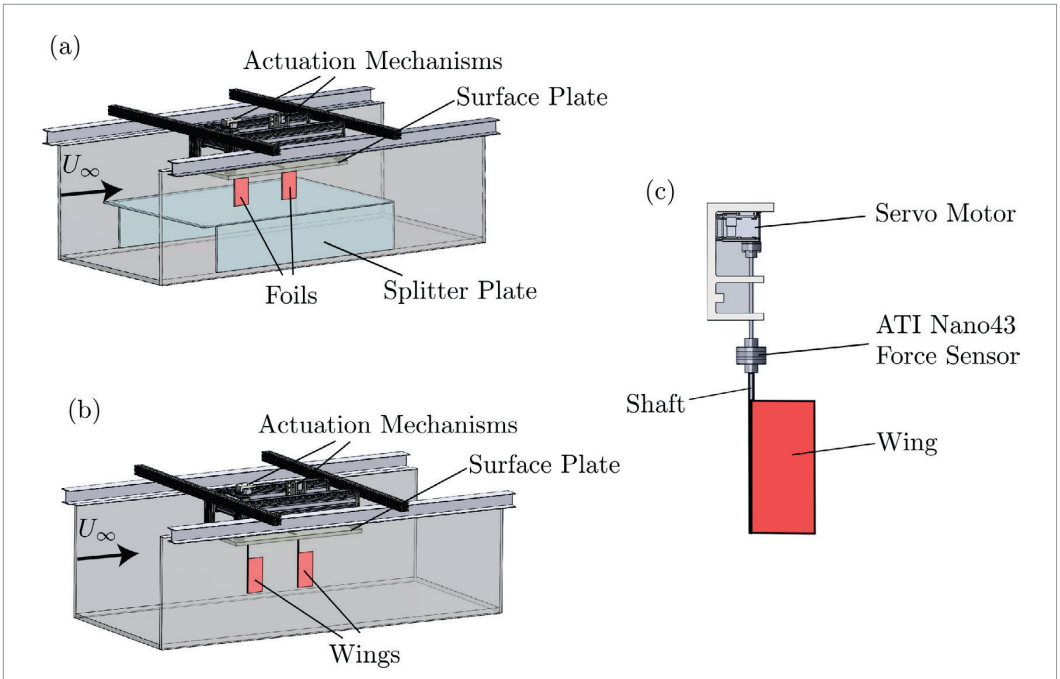

Figure 1. Schematic of the experimental setup showing (a) the two-dimensional, and (b) the three-dimensional configurations. The actuation mechanism is shown in (c).

plates thereby minimizing three-dimensional effects (figure 1(a)). In the three-dimensional configuration the splitter plate was removed and the wing was lowered to the mid-depth of the water tunnel (figure 1(b)).

Two identical wings designated as the leader and the follower were used for the experiments. Each wing had a rectangular planform shape, a chord length of $c = 0.095$ m, a span length of $s = 0.19$ m, and an aspect ratio of $AR = 2$. They were fabricated out of acrylonitrile butadiene styrene (ABS) and they had a teardrop cross-sectional shape [8, 25] with a thickness-to-chord ratio of $b/c = 0.07$ (figure 2). Each wing was pitched about its leading edge by a Dynamixel MX-64T servo motor while a US Digital E5 optical encoder tracked its angular position throughout the motion. The leader wing was pitched with a harmonic motion of $\theta_L(t) = \theta_0 \sin(2\pi ft)$ while the follower wing was pitched similarly as $\theta_F(t) = \theta_0 \sin(2\pi ft + \phi)$, where f is the frequency of the motion, t is the time, θ_0 is the amplitude of motion, and ϕ is the phase difference or *synchrony*. The synchrony between the wings was varied from $0 \leqslant \phi \leqslant 2\pi$ in increments of $\pi/12$ producing 24 phase differentials for each wing arrangement. Throughout this study the time will be non-dimensionalized by the period of motion as $t^* = ft$. The non-dimensional streamwise spacing between the wings, $X^* = X/c$, was varied from $0.25 \leqslant X^* \leqslant 1.25$ in 0.25 chord increments. The frequency of motion and pitching amplitude were held constant throughout the experiments at $f = 0.75$ Hz and $\theta_0 = 7.5°$, respectively. This gives a Strouhal number of $St = fA/U_\infty = 0.25$ and a reduced frequency of $k = fc/U_\infty = 1$, where $A = 2c \sin\theta_0$ is the peak-to-peak amplitude of motion. The input parameters for the current study can be found in table 1.

Pure pitching kinematics, as opposed to combined heaving and pitching, are used since pitching mechanisms are simple to fabricate, they are good models of pitch-dominated swimmers such as cod, saithe and trout, and they have been used in numerous bio-inspired studies [1, 8, 25–29]. The amplitude of motion is chosen to be $\theta_0 = 7.5°$ since for amplitudes of $\theta_0 \geqslant 8°$ a leading-edge vortex forms [28] and the efficiency performance of a pitching airfoil drops off [26, 28]. The Strouhal number of $St = 0.25$ is chosen since this leads to the peak propulsive efficiency for the isolated three-dimensional pitching wing with $\theta_0 = 7.5°$ (see section 3.1). This Strouhal number also falls within a range that is typical for high efficiency, bio-inspired propulsion [30–32]. Since the amplitude and St are fixed, the reduced frequency is also fixed by the definition, $k = St/(A/c)$. The synchrony and spacing of propulsors are chosen as the major variables of the current study since previous work has highlighted their prominent role in defining vortex-body interactions (see section 1). Future studies should probe the effects of varying the motion type, Strouhal number, and the non-dimensional amplitude.

An ATI Nano43 six-axis force sensor was used to measure the thrust, lift and pitching moments acting on the leader and follower wings. The instantaneous angular velocity of each wing was calculated by differentiating the angular position obtained from the optical encoder with a second-order central difference scheme. The instantaneous total input power was calculated as $P_T(t) = M_\theta \dot{\theta}$. Experiments were conducted

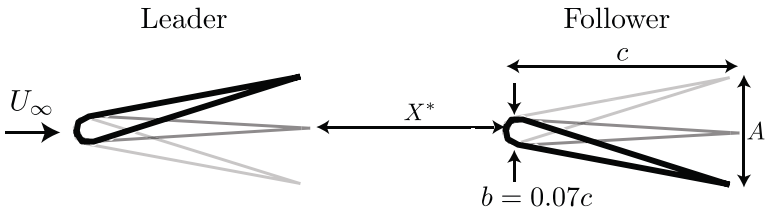

Figure 2. Geometric layout of the leader and follower propulsors.

Table 1. Experimental parameters used in the present study.

Parameters		
X^*	0.25–1.25	0.25 increments
ϕ	0–2π	$\pi/12$ increments
k	1	
St	0.25	
θ_0	7.5°	($A/c = 0.26$)

in air and the resultant inertial power data was subtracted from the total power data taken in the water tunnel to calculate the power input to the fluid, $P(t)$. The thrust, lift and power are reported as their mean values time-averaged over 100 oscillation cycles, which are denoted with an overbar such as $\overline{(\cdot)}$. The time-averaged values were measured over five trials and the mean values of the trials are reported for each set of parameters. The reported uncertainty is the standard deviation of the five time-average values. Typical uncertainties in the force, and power coefficients and efficiency measurements are ± 0.02, ± 0.004, and $\pm 3\%$, respectively. The coefficient of thrust, C_T, lift, C_L, and power, C_P, and the propulsive efficiency, η, for the leader or follower wings are defined as

$$C_T = \frac{\overline{T}}{\frac{1}{2}\rho U_\infty{}^2 cs}, \quad C_L = \frac{\overline{L}}{\frac{1}{2}\rho U_\infty{}^2 cs}, \quad C_P = \frac{\overline{P}}{\frac{1}{2}\rho U_\infty{}^3 cs}, \quad \eta = \frac{C_T}{C_P}, \tag{1}$$

where ρ is the fluid density.

In the current study we also report the collective performance, that is, the combined performance of the leader and follower wings. The collective performance is important when considering the performance enhancement from fin–fin interactions on the same swimmer, such as the dorsal-caudal fin interaction on fish, or in the design of bio-inspired devices with multiple fins or wings. The collective force and power coefficients as well as the collective efficiency are denoted with a C subscript and they are defined as

$$C_{T,C} = \frac{\overline{T}_L + \overline{T}_F}{\rho U_\infty{}^2 cs}, \quad C_{L,C} = \frac{\overline{L}_L + \overline{L}_F}{\rho U_\infty{}^2 cs}, \quad C_{P,C} = \frac{\overline{P}_L + \overline{P}_F}{\rho U_\infty{}^3 cs}, \quad \eta_C = \frac{C_{T,C}}{C_{P,C}}. \tag{2}$$

Note that the collective force and power coefficients use the combined wing planform area, that is $2cs$, cancelling the one-half in the denominator of the coefficient definitions. The force and power coefficients and the efficiency will be reported as normalized values that are compared to their equivalent isolated wing values. The normalized coefficients and efficiency are

$$C_T^* = \frac{C_T}{C_{T,iso}}, \quad C_L^* = \frac{C_L}{C_{L,iso}}, \quad C_P^* = \frac{C_P}{C_{P,iso}}, \quad \eta^* = \frac{\eta}{\eta_{iso}}. \tag{3}$$

Here the single wing metrics are compared to the values of a *single* isolated wing while the collective wing metrics are compared to the combined values of *two* isolated wings.

PIV data were acquired from the wakes of the foils/wings by employing an Imager sCMOS camera (2560 × 2160 pixels) and a 200 mJ/pulse Nd:YAG laser (EverGreen 200). The flow was seeded with 11 μm hollow metallic coated plastic sphere particles. At the beginning of each oscillation period a digital pulse signal was sent to the programmable timing unit (PTU) which triggers both camera and laser at the same time. The phase-averaged data was obtained for 24 discrete phases in oscillation cycle by averaging each discrete phase over 50 oscillation cycles. These 24 discrete phases averaged over 50 oscillation cycles were then used to acquire time-averaged flow fields. Four passes with two different window sizes were used in the vector calculations with a final interrogation window size of 32 × 32 pixels with 75% overlap. The uncertainty in the instantaneous velocity fields is estimated to be between 1%–5% [33].

3. Results

3.1. Isolated foil and wing

Measurements were made of an isolated two-dimensional foil and of an isolated three-dimensional wing. The coefficient of thrust, power and propulsive efficiency of the isolated foil and wing are reported in table 2. For the two-dimensional configuration two Reynolds numbers were tested in the current study at $Re = 4800$ and 7500. The high Reynolds number case had a reduced uncertainty in the efficiency as compared to the low Reynolds number case. Therefore, throughout the current study $Re = 7500$ is used, while the $Re = 4800$ case is for comparison with prior work reported in the table [1]. Note that the foil in the study of Boschitsch *et al* [1] also had a teardrop shape, was oscillated in a pitching motion with the same St and k, and had a slightly lower amplitude of $\theta_0 = 7.2°$.

Table 2. Propulsive performance of an isolated wing at $St = 0.25$ and $k = 1$ for both the two- and three-dimensional cases.

	Study	Re	C_T	C_P	η
2D	Boschitsch *et al* (2014)	4700	0.15 ± 0.02	0.66 ± 0.06	0.22 ± 0.04
2D	Present study	4800	0.14 ± 0.05	0.77 ± 0.001	0.18 ± 0.06
2D	Present study	7500	0.15 ± 0.02	0.79 ± 0.003	0.19 ± 0.02
3D	Present study	7500	0.21 ± 0.02	0.75 ± 0.005	0.28 ± 0.03

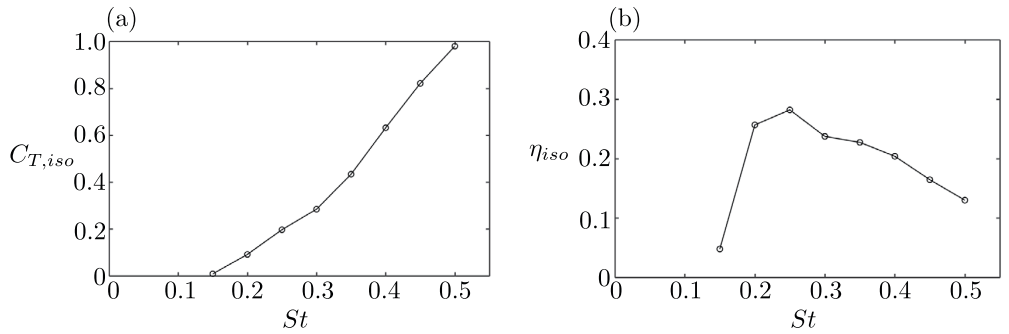

Figure 3. The thrust coefficient (a) and propulsive efficiency (b) of an isolated wing as a function of the Strouhal number.

In figure 3, the thrust coefficient and propulsive efficiency of an isolated wing at $Re = 7500$ are shown for a range of Strouhal number ($0.15 \leqslant St \leqslant 0.5$). As expected, thrust monotonically increases with increasing Strouhal number, whereas, propulsive efficiency peaks at $St = 0.25$ and thereafter monotonically decreases for the higher Strouhal numbers. Throughout the current study the Strouhal number is fixed at $St = 0.25$ since this leads to the peak efficiency of an isolated wing.

The mid-span vorticity field of the isolated foil and wing are shown in figure 4 at two non-dimensional times of $t^* = 0.25$ and 0.75, which occur at the maximum positive and negative pitching angles, respectively. Additionally, the vorticity fields at the mid- and quarter-span locations for the foil configuration where compared, which confirmed that indeed the vortex cores are aligned and the flow is nominally two-dimensional. Two oppositely signed vortices are shed from the trailing edge of the foil and the wing during each cycle producing a momentum surplus wake, indicative of thrust production, which is known as a reverse von Kármán vortex street. No leading-edge separation can be observed in two- or three-dimensional flows, although there is a small leading-edge vortex that forms and remains attached to the foil and wing as it propagates downstream as previously observed in two-dimensional DNS of a pitching NACA 0012 airfoil [28]. The wake vortices downstream of the three-dimensional wing can be seen to breakdown between $1 \leqslant x/c \leqslant 1.5$, which has been linked to the influence of the streamwise-oriented portions of the vortex rings shed from isolated pitching wings [34, 35]. In the wake of the foil, vortex breakdown also occurs, however, it occurs nearly twice as far downstream between $1.5 \leqslant x/c \leqslant 2$. This accelerated breakdown process in three-dimensional flows will be shown to lead to significant differences between the efficiency performance of in-line foils and wings.

3.2. Propulsive performance of the leader and follower

Here, we present the normalized thrust, power and efficiency of the leader and follower for the foils and wings. The novelty of the results is in the reporting of the performance of the three-dimensional interacting wings. The results of the two-dimensional interacting foils are used merely as a direct comparison for the three-dimensional results, and they are consistent with previously reported findings [1]. Figure 5 presents the performance coefficients of the leader as a function of the synchrony, ϕ, and spacing, X^*, between the propulsors. The performance of the two-dimensional foils and the three-dimensional wings show the same broad trends. At a fixed spacing, the performance varies periodically from minimum to maximum values as the temporal synchrony is varied. In fact, the power is observed to reach a minimum at $\phi = \pi$ and a maximum at $\phi = 0$, while the thrust reaches a maximum and minimum at $\phi = \pi/2$ and $\phi = 3\pi/2$, respectively. In accordance with Boschitsch *et al* [1], but in contrast to Broering *et al* [18], the thrust of the leader has a range of thrust enhancement and degradation as compared to an isolated propulsor. In general, for a fixed synchrony and increasing spacing the performance decays towards the isolated wing values. In contrast to the two-dimensional results, the normalized thrust for the wings varies over a smaller range and shows much lower values than that of the foils, even though the normalized power is approximately the same. This discrepancy further presents itself as a degradation in the normalized

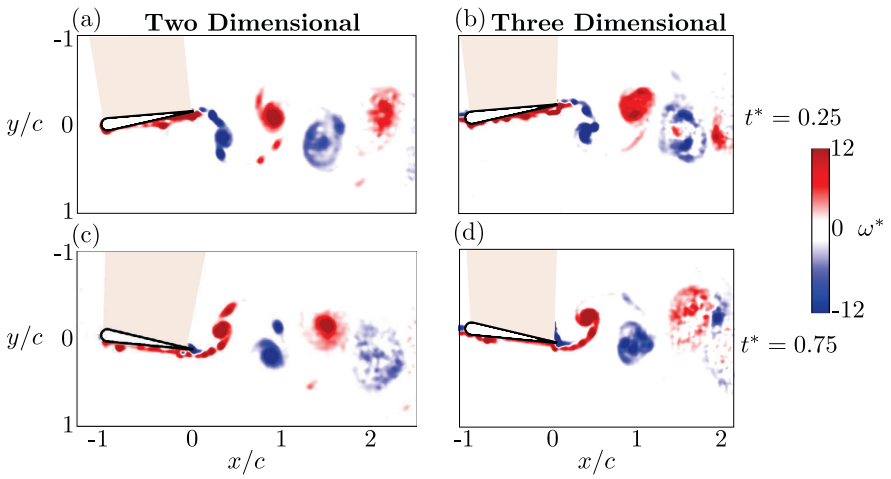

Figure 4. Instantaneous vorticity field in the wake of an oscillating foil ((a) and (c)) and a wing ((b) and (d)) are shown at $t^* = 0.25$ and 0.75. The flow field measurements are taken at the mid-span of the propulsors.

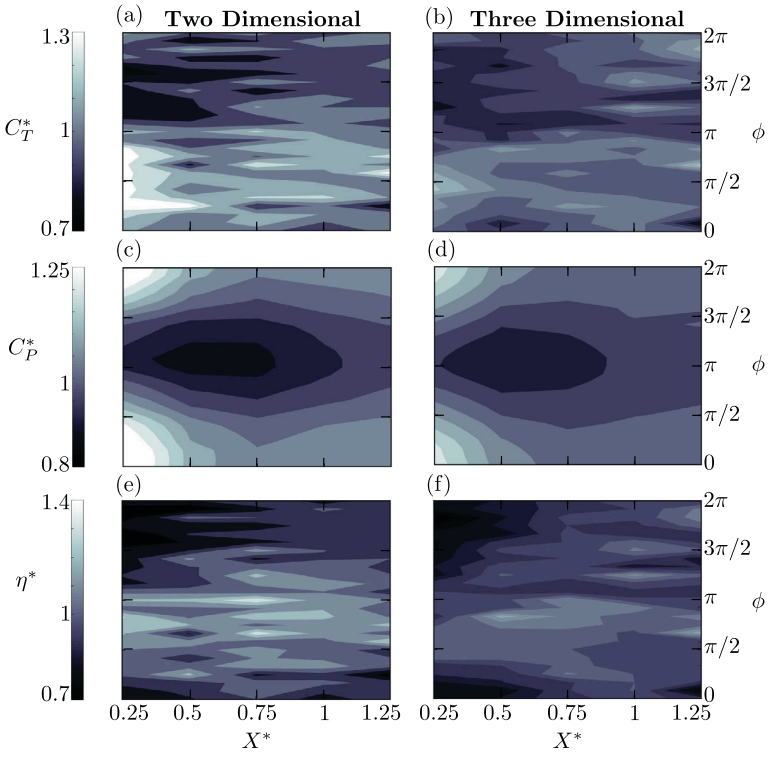

Figure 5. Normalized thrust, and power coefficients and propulsive efficiency of the two-dimensional leader foil (left) and the three-dimensional leader wing (right).

efficiency from a maximum of a 30% normalized efficiency increase for the foils to a maximum of a 5% increase for the wings at the closest spacing of $X^* = 0.25$.

Figure 6 presents the normalized thrust, power and efficiency of the follower as a function of the synchrony and spacing. The striking band structures that were first reported in the study of Boschitsch [1] for in-line foils, can be observed in not only two-dimensional interactions here, but also in three-dimensional interactions. This is expected though since the performance of the follower is highly dependent upon the synchrony between the propulsor motion and the impinging vortex street, which can be described as a *spatial* instead of temporal synchrony as, $\phi_{spatial} = \phi - 2\pi X^*/\lambda^*$, [36, 37]. Here λ^* is the wake vortex wavelength normalized by the chord length of the propulsors. By examining the slopes of the bands the vortex wake wavelength and the vortex advection speed can

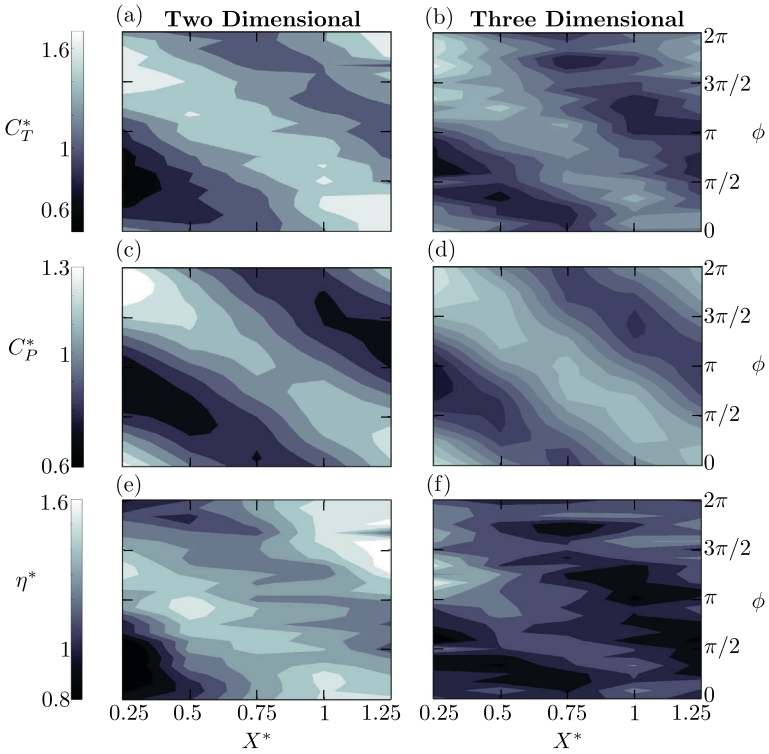

Figure 6. Normalized thrust, and power coefficients and propulsive efficiency of the two-dimensional follower foil (left) and the three-dimensional follower wing (right).

be inferred. The two-dimensional data admits a wake wavelength of $\lambda^* = 1.2$ and a vortex advection speed of $U_{adv} = 1.2\ U_\infty$ as reported previously [1], while the three-dimensional data admits a wake wavelength of $\lambda^* \approx 1.02$ and vortex advection speed of $U_{adv} = 1.02\ U_\infty$. The same wake wavelengths can be measured from the mid-span PIV data for the *isolated* propulsors suggesting that the downstream propulsor has little influence on the timing of impingement of the vortices. However, the timing of vortex impingement *is* altered between the two- and three-dimensional cases. This is expected since it is well-known that the propagation speed of a two-dimensional vortex pair is greater than that of an equivalent three-dimensional closed loop vortex ring.

By comparing the performance of the follower foil and wing it is clear that the reduced efficiency performance of the wing can be attributed to its lower thrust gains across the parameter space. In contrast, the peak normalized power coefficients of the two- and three-dimensional cases are quite similar. Additionally, it should be noted that the normalized power coefficient of the follower foil varies between $0.6 \leqslant C_P^* \leqslant 1.3$ (figure 6(c)) as compared to previous findings [1] where it varied between $0.9 \leqslant C_P^* \leqslant 1.1$. This difference between the two studies may be attributed to the difference in the Reynolds numbers, although no direct evidence of this is presented. However, this argument is supported by the increase in power consumption observed in the isolated foil as the Reynolds number increases (section 3.1).

3.3. Modes of interaction and flow mechanisms

Previously it was proposed that two interaction modes exist between *two-dimensional* in-line propulsors: a coherent and a branched interaction mode [1]. The coherent mode forms a single-core momentum jet or a 'coherent jet' in the time-average and was previously linked to peak thrust production and peak *efficiency* of the follower. The branched mode forms a dual-core momentum jet or a 'branched jet' in the time-average and was linked to the minimum power consumption and minimum *efficiency* of the follower. Here, we will show that the interaction modes extend to *three-dimensional* interactions. Additionally, we will demonstrate that while the coherent mode occurs at peak thrust production and the branched mode occurs at the minimum power consumption, the modes are *not* found to be directly linked to the propulsive efficiency, even in *two-dimensional* interactions.

Figure 7 presents a time series of the vorticity field at $X^* = 0.25$ and $\phi = 7\pi/4$ for the foils and the wings. These parameters are near the peak thrust conditions for both propulsor types. For the foils and wings, at $t^* = 0$ a negative vortex shed from the leader impinges on the leading edge of the follower as it is moving upward through $\theta = 0$. As previously proposed, the vortex impinges on the suction side of the propulsor thereby enhancing its leading-edge suction and consequently its thrust production [1]. The impinging vortex induces a separating shear layer, which by $t^* = 0.25$ has rolled up into a leading-edge vortex and

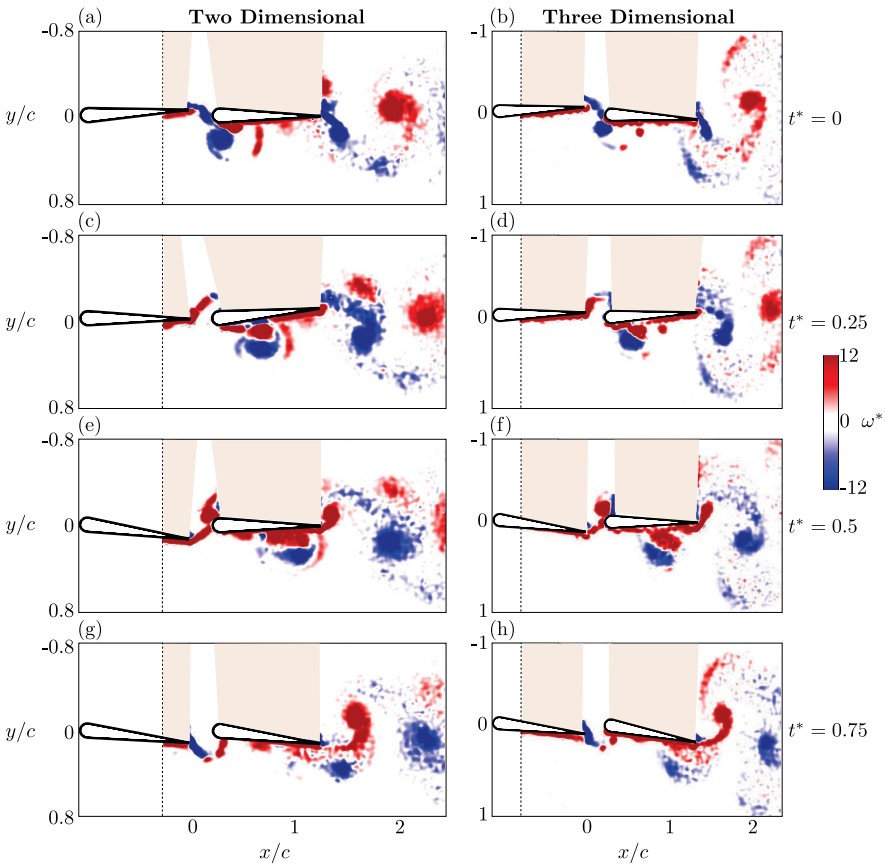

Figure 7. Time series of the vorticity field at $X^* = 0.25$ and $\phi = 7\pi/4$ for the foils (left) and the wings (right). These cases are near the peak thrust conditions for both propulsor types.

the two pair-up to form a vortex dipole. In the case of the foils, the vortex dipole is oriented almost directly downstream, while in the case of the wings it is oriented more in the lateral direction, thereby slowing its downstream propagation. By $t^* = 0.5$ the vortex dipole has traveled in the streamwise direction along the surface of the propulsor in both cases. The vortex dipole in the case of the foils has reached the trailing-edge between $t^* = 0.5$ and $t^* = 0.75$, and the separated vortex is absorbed into the forming trailing-edge vortex, increasing its strength. In the case of the wings the vortex dipole does not reach the trailing edge until $t^* = 0.75$ where the separated vortex is also absorbed into the forming trailing-edge vortex. Except for the above-mentioned differences in the midspan data the vortical interactions leading to the peak thrust condition in three-dimensional interactions is consistent with the findings reported on two-dimensional interactions [1, 15].

Figure 8 presents a time series at $X^* = 0.25$ and $\phi = 5\pi/6$ that is near the minimum power conditions for the foils and wings. At $t^* = 0$ a negative vortex shed from the leader impinges on the lower surface of the follower as it is moving downward through $\theta = 0$. The impinging vortex induces a separated leading-edge vortex on the pressure side thereby counteracting the leading-edge suction on the suction side and consequently lowering its lift and power consumption, as previously proposed [1]. At $t^* = 0.25$ the impinging and separated vortices have paired into a dipole that is propagating laterally away from the foil with a small downstream orientation but in the three-dimensional case the orientation of the dipole is almost normal to the surface of the propulsor with little or no downstream orientation. By $t^* = 0.5$ the dipole is located above the mid-chord, while for the peak thrust condition the dipole had reached the trailing-edge indicating that in the minimum power case the dipole is propagating downstream with approximately half the speed. At the same time, there is a forming trailing-edge vortex from the follower. Between $t^* = 0.75$ and $t^* = 0$ the vortex dipole has reached the trailing edge and in the case of the three-dimensional wings the dipole is breaking down. Based on the midspan data, the vortical interactions leading to the minimum power condition in three-dimensional propulsors are nearly identical to those reported for two-dimensional foils [1].

Previously, for the peak thrust condition a single-core momentum jet formed downstream of the follower foil in the time-average. This condition was described as the 'coherent' interaction mode and it

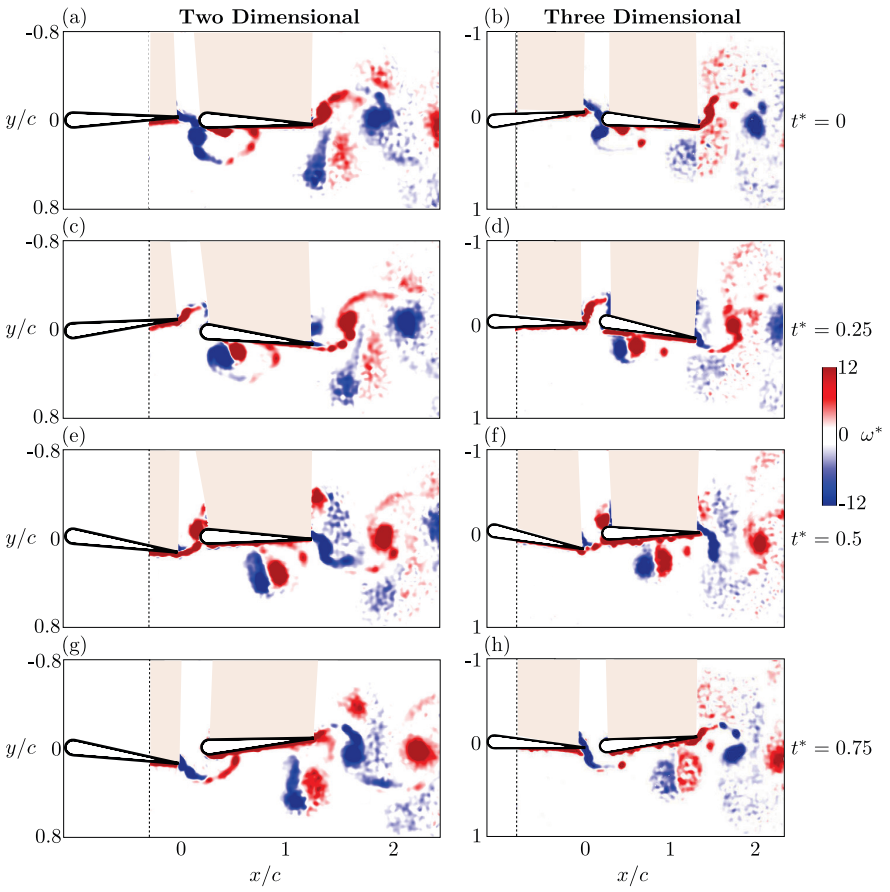

Figure 8. Time series of the vorticity field at $X^* = 0.25$ and $\phi = 5\pi/6$ for the foils (left) and the wings (right). These cases are near the minimum power conditions for both propulsor types.

was further proposed that peak efficiency occurred for this mode [1]. Similarly, for the minimum power condition a dual-core momentum jet formed downstream of the follower foil in the time-average. This condition was described as the 'branched' interaction mode and it was further proposed that minimum efficiency occurred for this mode. Figure 9 presents the time-averaged x-component of velocity for two- and three-dimensional flows at $X^* = 0.25$, 0.75, and 1.25 at peak thrust and minimum power conditions. Here, it can be observed that indeed the coherent and branched interaction modes are present in the two-dimensional interactions, and importantly the same interaction modes are recovered in the three-dimensional interactions. Also, note that these interaction modes are invariant with the spacing.

In contrast to previous findings [1], the interaction modes *do not* indicate a maximum or minimum in propulsive efficiency. For example, peak efficiency for the follower propulsor at $X^* = 0.25$ and at $X^* = 0.75$ reveal a branched wake mode and a coherent wake mode, respectively (figure 10), in two-dimensional flows. The same conclusion can be made for the follower peak efficiency cases in three-dimensional flows (figure 10) with small alterations in the interaction mode at $X^* = 0.75$ due to earlier vortex breakdown in three dimensions (see figure 4). The interaction modes in both two- and three-dimensional flows *do* indicate that the peak efficiency condition at $X^* = 0.25$ is closer to its minimum power condition than its peak thrust condition and *vice versa* for $X^* = 0.75$. These results can be understood by considering that the efficiency is just the ratio of the thrust and power coefficients. Therefore peak efficiency should be attainable by either minimizing the power or maximizing the thrust, or a combination of both. In fact, the combination case is exactly what is occurring in the $X^* = 0.25$ case. It is likely that the discrepancy between the current study and the previous findings [1] is due to the Reynolds number difference. The higher Reynolds number of the current study is correlated with a larger variation in the power coefficient making its contribution to the peak efficiency conditions more prominent. Yet, in general it can be concluded that peak efficiency is not associated with the coherent or branched interaction modes, only peak thrust and minimum power, respectively.

3.4. Propulsive performance of the collective

Figure 11 presents the normalized thrust, power, efficiency, and lift of the collective for two- and

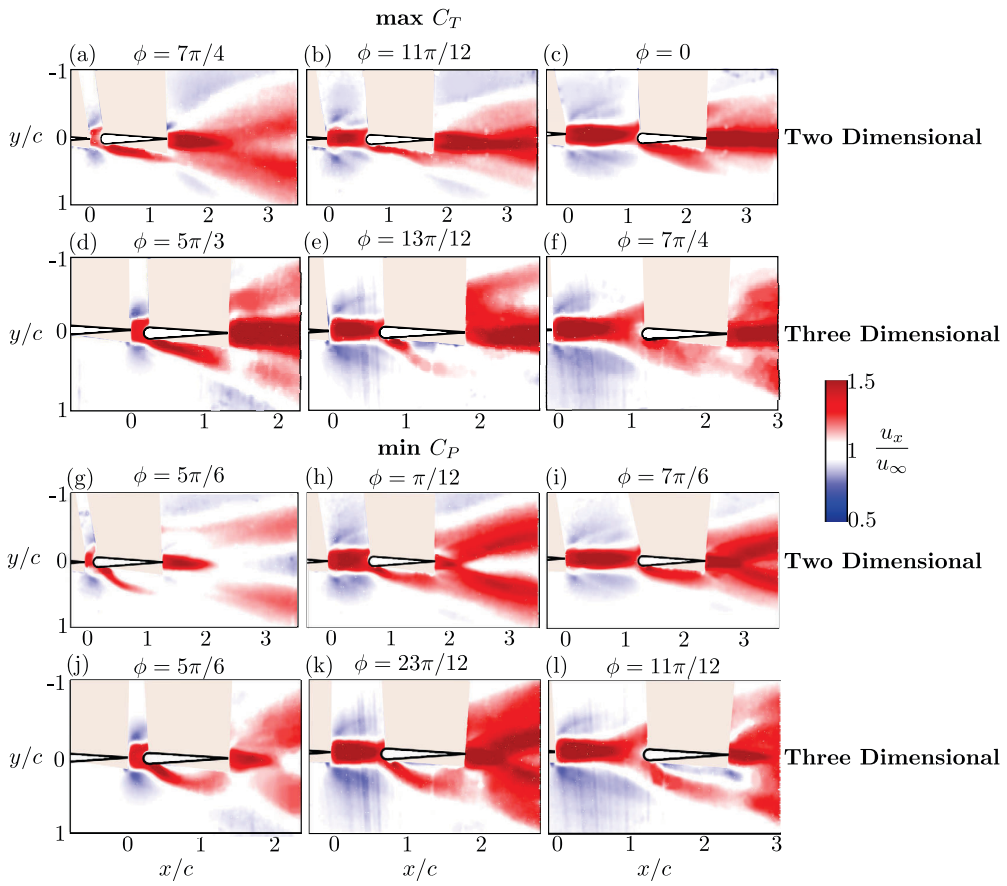

Figure 9. The time-averaged x-component of velocity for two- and three-dimensional flows at $X^* = 0.25, 0.75$, and 1.25 at peak thrust and minimum power conditions. The phase difference for each case is indicated at the top of each of the images.

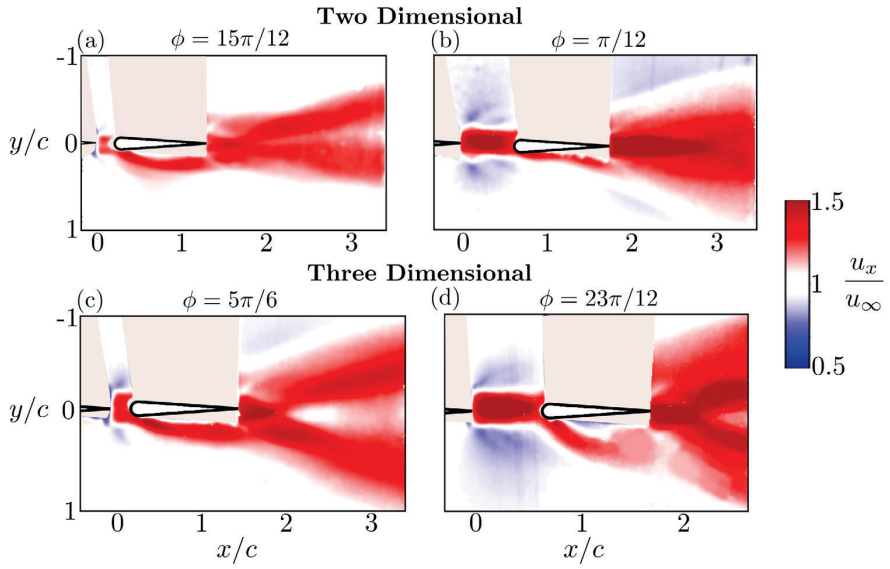

Figure 10. The time-averaged x-component of velocity for two- and three-dimensional flows at $X^* = 0.25$ ((a) and (c)) and 0.75 ((b) and (d)), at the peak efficiency conditions for the follower.

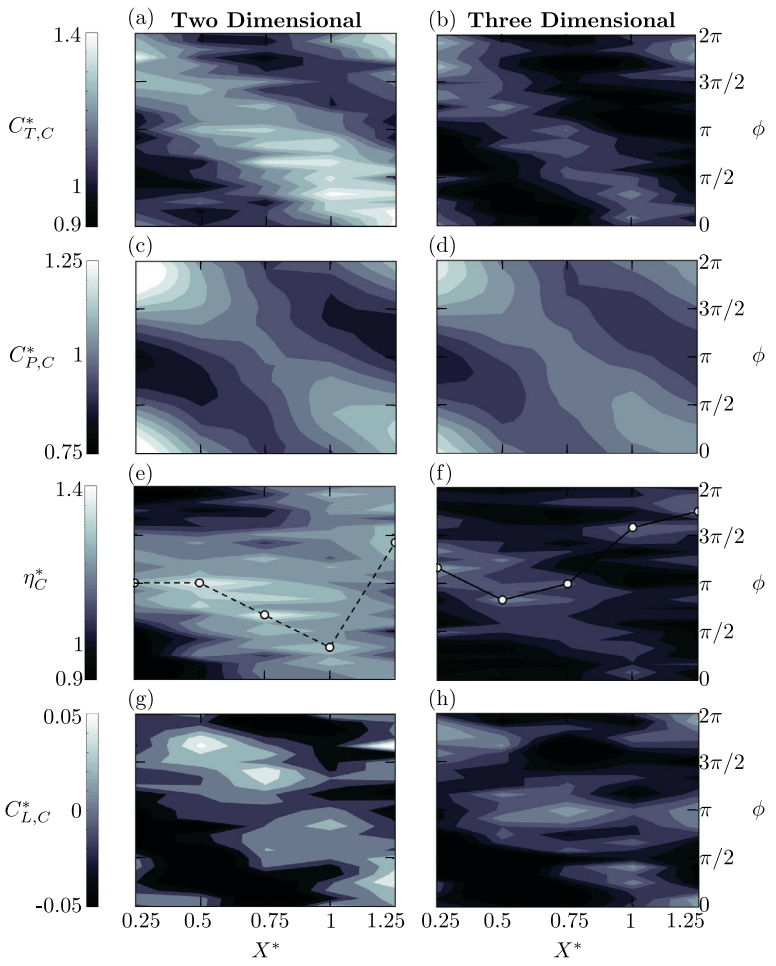

Figure 11. Normalized collective thrust, power, and lift coefficients and collective efficiency of two-dimensional (left) and three-dimensional (right) cases. The circle markers in (e) and (f) connected by the dashed lines represent the points of maximum attainable efficiency at each spacing.

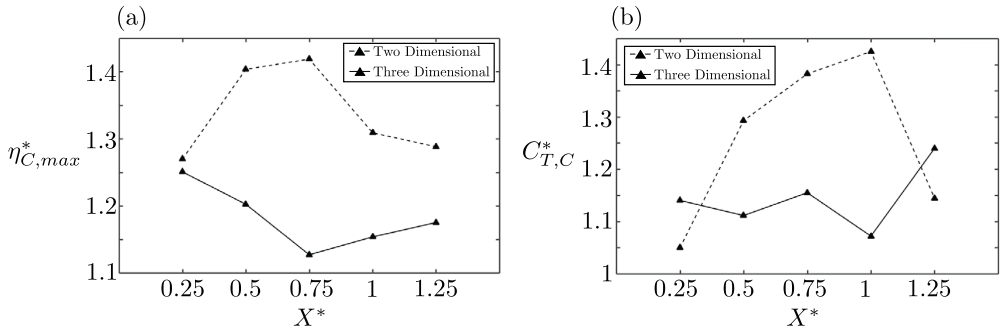

Figure 12. (a) Maximum attainable normalized collective efficiency as a function of spacing and (b) corresponding normalized collective thrust as a function of spacing. The dashed and solid lines represent the two- and three-dimensional cases, respectively.

three-dimensional flows as a function of the synchrony and streamwise spacing. It is striking how similar the broad trends are between the follower and the collective in thrust, power and efficiency clearly indicated by similar prominent band structures. This similarity suggests that the follower performance is the main driver of the collective performance with moderate modifications due to the leader as proposed previously [1]. In general, the similarities and differences between the two- and three-dimensional data follow the follower data discussion in section 3.2 with the exception of (1) the maximum attainable efficiency at each spacing and (2) the collective lift data.

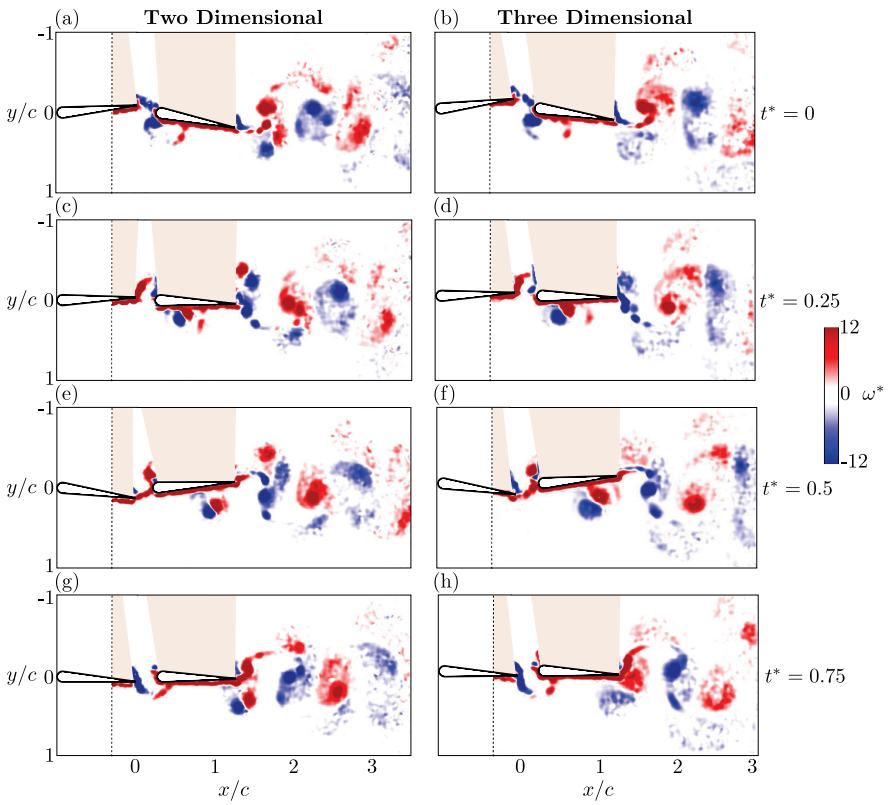

Figure 13. Time series of the vorticity field at $X^* = 0.25$ and $\phi = 7\pi/6$ for two-dimensional (left) and three-dimensional (right) collectives. These conditions are near peak efficiency conditions for both collectives.

The *key difference* between two- and three-dimensional in-line interacting propulsors is in their collective maximum attainable efficiency. At a given spacing the maximum efficiency across all of the synchronies is defined as the maximum attainable efficiency, η^*_{max}, at that spacing. In figures 11(e) and (f), the markers connected by the dashed lines represent the maximum attainable normalized collective efficiency at each spacing. These data are then graphed in figure 12(a) along with their associated normalized thrust coefficients in figure 12(b). It is revealed that in two-dimensional interactions the maximum attainable efficiency increases to an optimal point at $X^* = 0.75$ with $\phi = 2\pi/3$ and $\eta^*_{C,max} = 1.42$, and then decreases with a further increase in spacing. In contrast, the three-dimensional interactions have an optimal maximum attainable efficiency at $X^* = 0.25$ with $\phi = 7\pi/6$ and $\eta^*_{C,max} = 1.25$, and decrease with increasing spacing until $X^* = 0.75$ where it then increases beyond that spacing. The three-dimensional data shows the exact opposite trend in the maximum collective efficiency as compared to the two-dimensional data. In fact, if two-dimensional data is used to determine the optimal spacing of the leader and follower for three-dimensional wings then the worst possible case would be chosen. This reveals that there are actually significant qualitative differences between two- and three-dimensional interactions that must be considered. Along with the efficiency gains at the optimal spacing and synchrony, the two- and three-dimensional data also show collective thrust gains of 38% and 15%, respectively (12(b)).

For the first time, the collective lift for in-line interacting foils and wings is reported in figure 11. The collective lift varies from positive to negative values with band structures that are offset from the thrust or power bands. Surprisingly, at the maximum attainable efficiency points the collective lift is effectively zero. It is unclear whether this is true for all interacting configurations, however, we can postulate that by reducing the collective lift to zero the lateral waste kinetic energy in the wake is likely minimized, which could lead to a maximum in efficiency. However, further study is needed to examine this conjecture.

3.5. Two- and three-dimensional collective wake interactions

In order to understand why the collective efficiency gains in two- and three-dimensions show the opposite trends with increasing spacing, the wake interactions were measured. Time series for two- and three-dimensional wake measurements are compared at $X^* = 0.25$ in figure 13 and at $X^* = 0.75$ in figure 14. The synchronies of the $X^* = 0.25$ and $X^* = 0.75$ cases were chosen to coincide with the optimal maximum collective efficiency of the wings ($\phi = 7\pi/6$) and foils ($\phi = 2\pi/3$), respectively.

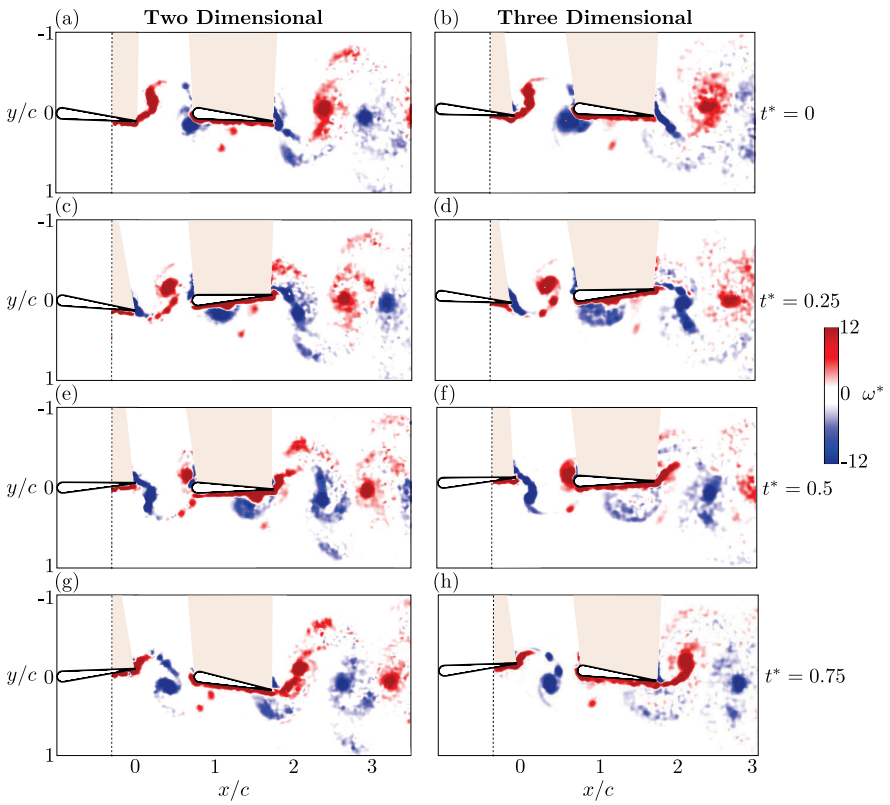

Figure 14. Time series of the vorticity field at $X^* = 0.75$ and $\phi = 2\pi/3$ for two-dimensional (left) and three-dimensional (right) collectives. These conditions are near peak efficiency conditions for both collectives.

Figure 13 presents wake measurements at the mid-span of the propulsors for a spacing of $X^* = 0.25$. For the closely spaced foils and wings the vortex dynamics are observed to be quite similar in two- and three-dimensions. The vortex dynamics in both cases follow the description given in section 3.3 detailing the minimum power modal interaction. There are only a few small differences between the two- and three-dimensional cases. In the case of the interacting wings the vortex dipole is oriented more towards the streamwise direction than the interacting foils case. Additionally, the vortex dipole in the three-dimensional case begins to breakdown by $t^* = 0.75$ and is almost indistinguishable by $t^* = 0$, in contrast to the two-dimensional case. These differences are relatively minor and consequently the efficiency performance of the two- and three-dimensional cases are nearly identical (figure 12). However, the three-dimensional case shows a 15% gain in thrust as compared to two wings in isolation while the two-dimensional case shows a 5% gain in thrust. This is likely due to the absorption of the separated leading-edge vortex into the forming trailing-edge vortex system at $t^* = 0.75$ in the three-dimensional case, but not in the two-dimensional case. This strengthening of the forming momentum jet does not occur until nearly one chord length downstream in the two-dimensional case minimizing its influence on the forces acting on the follower wing.

Figure 14 presents wake measurements at the mid-span of the propulsors for a spacing of $X^* = 0.75$. For this spacing the foils have higher efficiency and thrust gains than at $X^* = 0.25$. This increased performance is associated with the alignment of the peak efficiency case more closely with the peak thrust modal interaction as can be observed from the two-dimensional vortex dynamics. In contrast, the three-dimensional case has a lower efficiency gain at $X^* = 0.75$ than at $X^* = 0.25$ even though the vortex dynamics are similar in nature to the peak thrust modal interaction. However, there is a major difference between the two- and three-dimensional cases. In the three-dimensional case the impinging vortex at $t^* = 0$ has a core size that is nearly twice as large as the two-dimensional case and as time progresses the impinging vortex is observed to breakdown over the surface of the follower wing. Consequently, at the mid-span the impinging vortex has a diminished effect on the follower wing, which is evident from the nearly non-existent induced leading-edge vortex at $t^* = 0.5$ and 0.75 in contrast to the two-dimensional case. The weaker influence at the mid-span on the follower wing correlates with the decreasing efficiency performance as the spacing is increased between the leader and follower. This accelerated vortex breakdown has been linked to the influence of the tip portions of the shed vortex loops [35] and may be further accelerated by the spanwise

pressure gradients over the surface of the follower that occurs in finite-span wings [34, 38]. This three-dimensional mechanism has only been examined at the mid-span of the wing and therefore offers a simple correlation with the performance data. Future work should focus on revealing the full three-dimensional vortex-body interactions to gain a deeper understanding of this breakdown mechanism.

4. Conclusions

We have presented new experiments examining the role of three-dimensional effects on the interactions of two pitching propulsors in an in-line configuration. Force and flow measurements show that two-dimensional foils and three-dimensional wings have many broad similarities. In three-dimensional interactions, as previously found in two-dimensional interactions [1], the leader performance depends on the temporal synchrony while the follower performance depends on the spatial synchrony giving rise to band structures in the performance data. Furthermore, PIV measurements reveal that in three-dimensional interactions the peak thrust and minimum power interaction modes are nearly identical to those discovered for two-dimensional interactions [1], which in the time average are described as the coherent and branched modes, respectively. In contrast to previous work [1], it is demonstrated that the coherent and branched interaction modes *do not* correlate with maximum and minimum gains in propulsive efficiency, but instead coincide with only peak thrust and minimum power, respectively.

Beyond these broad similarities, there are several differences between the interaction of the foils and wings. First, the slopes of the bands in the performance data are different indicating that the vortex advection speed is $U_{adv} = 1.2U_\infty$ in the wake of the foils, consistent with previous findings [1], while it is $U_{adv} = 1.02U_\infty$ in the wake of the wings. This leads to different timing in terms of vortex impingement in two- and three-dimensional flows. Second, three-dimensional collective performance shows an attenuation in the normalized efficiency where the maximum collective efficiency of the wings is 25% higher than two wings in isolation while for the foils the maximum collective efficiency gain is 42%. This occurs due to overall higher normalized power for the wings than the foils, while the normalized thrust remains nearly the same between the foils and wings. Finally, the interacting foils and wings show the opposite trend in the maximum attainable collective efficiency as a function of the spacing. As the spacing increases, the foils maximum collective efficiency gain increases, while the wings maximum collective efficiency gain decreases. This difference is correlated to the breakdown of the impinging vortex on the mid-span of the follower wing in three-dimensional flows. For the interacting foils an optimal collective efficiency gain of 42% and a concurrent thrust gain of 38% occurs at $X^* = 0.75$ and $\phi = 2\pi/3$, while for the interacting wings an optimal collective efficiency gain of 25% and a concurrent thrust gain of 15% occurs at $X^* = 0.25$ and $\phi = 7\pi/6$.

The current results provide a framework for designing networked bio-inspired control elements that operate in three-dimensions. The results indicate that from a sensing perspective it is crucial to be able to detect the impingement of a vortex in order to properly synchronize interacting control elements either on the same vehicle or in a school of vehicles. Moreover, being able to further detect when wake breakdown occurs can help tailor, through feedback control, the optimal spacing between propulsive control elements. Further work is needed to integrate the three-dimensional flow physics information discovered in this work into the design of a closed-loop feedback control system for networked bio-inspired control elements.

Acknowledgments

This work was supported by the National Science Foundation under Program Director Dr. Ronald Joslin in Fluid Dynamics within CBET on NSF award number 1653181. Some of this work was also funded by the Office of Naval Research under Program Director Dr Robert Brizzolara on MURI grant number N00014-08-1-0642.

ORCID iDs

Melike Kurt https://orcid.org/0000-0001-6711-7025
Keith W Moored https://orcid.org/0000-0002-4331-3774

References

[1] Boschitsch B M, Dewey P A and Smits A J 2014 *Phys. Fluids* **26** 051901
[2] Wynne-Edwards V C 1962 Animal dispersion: in relation to social behaviour *Technical Report* (Edinburgh: Oliver & Boyd)
[3] Tinbergen J 2012 *Social Behaviour in Animals: with Special Reference to Vertebrates* (Berlin: Springer)
[4] Weihs D 1973 *Nature* **241** 290–1
[5] Becker A D, Masoud H, Newbolt J W, Shelley M and Ristroph L 2015 *Nat. Commun.* **6** 8514
[6] Lighthill M 1971 *Proc. R. Soc.* B **179** 125–38
[7] Tuncer I H and Kaya M 2003 *J. Aircr.* **40** 509–15
[8] Quinn D B, Moored K W, Dewey P A and Smits A J 2014 *J. Fluid Mech.* **742** 152–70
[9] Drucker E G and Lauder G V 2001 *J. Exp. Biol.* **204** 2943–58
[10] Standen E and Lauder G V 2007 *J. Exp. Biol.* **210** 325–39
[11] Partridge B L, Pitcher T, Cullen J M and Wilson J 1980 *Behav. Ecol. Sociobiol.* **6** 277–88
[12] Shoele K and Zhu Q 2015 *Bioinspir. Biomim.* **10** 026008
[13] Maertens A P, Gao A and Triantafyllou M S 2017 *J. Fluid Mech.* **813** 301–45
[14] Gopalkrishnan R, Triantafyllou M, Triantafyllou G and Barrett D 1994 *J. Fluid Mech.* **274** 1–21
[15] Akhtar I, Mittal R, Lauder G V and Drucker E 2007 *Theor. Comput. Fluid Dyn.* **21** 155–70
[16] Rival D, Hass G and Tropea C 2011 *J. Aircr.* **48** 203–11
[17] Broering T M, Lian Y and Henshaw W 2012 *Am. Inst. Aeronaut. Astronaut. J.* **50** 2295–307

[18] Broering T M and Lian Y S 2012 *Acta Mech. Sin.* **28** 1557–71
[19] Gong W Q, Jia B B and Xi G 2015 *Am. Inst. Aeronaut. Astronaut. J.* **53** 1693–705
[20] Gong W Q, Jia B B and Xi G 2016 *Exp. Fluids* **57** 8
[21] Muscutt L, Weymouth G and Ganapathisubramani B 2017 *J. Fluid Mech.* **827** 484–505
[22] Warkentin J and DeLaurier J 2007 *J. Aircr.* **44** 1653–61
[23] Daghooghi M and Borazjani I 2015 *Bioinspir. Biomim.* **10** 056018
[24] Liu G, Ren Y, Dong H, Akanyeti O, Liao J C and Lauder G V 2017 *J. Fluid Mech.* **829** 65–88
[25] Godoy-Diana R, Aider J L and Wesfreid J E 2008 *Phys. Rev.* E **77** 016308
[26] Buchholz J H and Smits A J 2008 *J. Fluid Mech.* **603** 331–65
[27] Dewey P A, Quinn D B, Boschitsch B M and Smits A J 2014 *Phys. Fluids* **26** 041903
[28] Das A, Shukla R K and Govardhan R N 2016 *J. Fluid Mech.* **800** 307–26
[29] Fernandez-Prats R 2017 *Ocean. Eng.* **145** 24–33
[30] Triantafyllou M S, Techet A H and Hover F S 2004 *IEEE J. Ocean. Eng.* **29** 585–94
[31] Taylor G K, Nudds R L and Thomas A L 2003 *Nature* **425** 707–11
[32] Saadat M, Fish F E, Domel A, Di Santo V, Lauder G and Haj-Hariri H 2017 *Phys. Rev. Fluids* **2** 083102
[33] Sciacchitano A, Wieneke B and Scarano F 2013 *Meas. Sci. Technol.* **24** 045302
[34] Green M A and Smits A J 2008 *J. Fluid Mech.* **615** 211–20
[35] Green M A, Rowley C W and Smits A J 2011 *J. Fluid Mech.* **685** 117–45
[36] Portugal S J, Hubel T Y, Fritz J, Heese S, Trobe D, Voelkl B, Hailes S, Wilson A M and Usherwood J R 2014 *Nature* **505** 399–402
[37] Epps B P, Muscutt L, Roesler B, Weymouth G and Ganapathisubramani B 2016 *J. Ship Prod. Des.* **33** 276–82
[38] McKenna C, Bross M and Rockwell D 2017 *J. Fluid Mech.* **816** 306–30